https://doi.org/10.5194/egusphere-2026-4384
Preprint. Discussion started: 4 August 2026

Frontal Coupling Regulated by Mesoscale Eddies in the Subarctic Frontal Zone

Aoran Sun[1], Chunling Zhang[1], Huangxin Yang[1], Yuntao Zhou[2]

[1]College of Marine Science, Shanghai Ocean University, Shanghai, China
[2]School of Oceanography, Shanghai Jiao Tong University, Shanghai, China

Correspondence to: Chunling Zhang (clzhang@shou.edu.cn), Yuntao Zhou (ytzhou@sjtu.edu.cn)

Abstract. Frontal coupling and its interaction with mesoscale eddies plays a critical role in water mass exchange and the ecodynamic balance in the Subarctic Frontal Zone of the northwestern Pacific. Using ten years (2014-2023) of daily satellite observations, this study systematically investigates the coupling characteristics of temperature and chlorophyll fronts under eddy modulation, along with the spatiotemporal responses of frontal coupling to eddy evolution by eddy partitioning, normalization, and lagged cross-correlation and mediation analyses. The eddy modulation on temperature and chlorophyll-a fronts pronouncedly depend on eddy polarity and developmental stage. Cyclonic eddies enhance chlorophyll-a fronts in the eddy core and concentrate temperature fronts at their periphery, whereas anticyclonic eddies suppress both frontal types in the core with recovery in the exterior. Under cyclonic eddy perturbation, the probability of frontal coupling increases with eddy intensity. The optimal lag time is 3-8 days, and the coupling probability in the eddy core is much higher than that of exterior. Anticyclonic eddies show a weaker promoting effect that is inversely related to eddy intensity, with a lag time of longer than 10 days. The responses of the two frontal types to eddy forcing are asynchronous. There is a time lag of several to over ten days between the physical-biological frontal coupling and eddy generation. While temperature fronts play a significant mediating role in this process, the mediation mechanisms differ according to eddy dynamic parameters and lag time. These findings demonstrate that eddy polarity and intensity jointly determine the direction, magnitude and duration of frontal coupling. That will provide a better understanding for the coupled mechanisms between physical and ecological fronts, as well as the oceanic dynamical and biological responses to eddy modulation.

1 Introduction

Oceanic fronts are narrow transition zones characterized by sharply enhanced horizontal gradients in physical and biogeochemical properties. They represent global hotspots where multi-scale dynamical processes and ecosystem interactions converge (Belkin et al., 2009). Warm and saline Kuroshio water converges with cold and fresh Oyashio water to form a pronounced subarctic frontal zone in the subarctic Northwest Pacific (Chelton et al., 2011; Qiu et al., 2014). This region hosts vigorous mesoscale and submesoscale activity. Where cyclonic and anticyclonic eddies are continuously generated, propagate, and dissipate. Their spatial scales are tens or hundreds of kilometers with lifetime of weeks to months, interacting strongly with the background fronts. Frontal dynamics associated with temperature in fronts transport nutrient-rich subsurface waters into the euphotic zone through vertical pumping and secondary circulations. This nutrient supply fuels phytoplankton growth, creates localized productivity maxima and frequently produces distinct chlorophyll-a (Chl-a) fronts (Calil and Richards, 2010; Taylor and Ferrari, 2011; Moline, 2014; Woodson and Litvin, 2015; Guo et al., 2022). Temperature fronts and Chl-a fronts, however, do not always coincide spatially. Temperature fronts are governed primarily by physical processes, whereas Chl-a fronts emerge from the combined effects of physical transport and biological growth. The coupling between these two frontal types is subject to modulation by multiple dynamical processes, with mesoscale eddies playing a particularly critical role.

https://doi.org/10.5194/egusphere-2026-4384
Preprint. Discussion started: 4 August 2026

Mesoscale eddies are ubiquitous dynamical processes in the ocean, occupying approximately 25% of the global ocean surface (Chaigneau et al., 2009). These eddies serve as a critical bridge between large-scale circulation and local oceanic properties, substantially modifying nutrient supply and phytoplankton distribution in the upper layer through horizontal advection and vertical pumping (Gaube et al., 2014; McGillicuddy, 2016). These processes play an essential role in material transport, energy cascade and biogeochemical cycling (Gaube et al., 2014; McGillicuddy, 2016). Eddies and fronts interact through two-way dynamical pathways. The rotation of eddies can meander and fragment background fronts, intensifying local horizontal gradients in phytoplankton biomass (Siegel et al., 2011). Conversely, frontal instability can trigger eddy shedding, which in turn modifies the structure and intensity of existing temperature fronts (Ribbe et al., 2018). In the central subarctic Pacific, eddies shed from the Alaskan Stream exert a substantial influence on Chl-a distribution (Ueno et al., 2010). And mesoscale eddies interact with temperature frontal variability to shape the seasonal Chl-a cycle in the Kuroshio Extension (Sasai et al., 2010). Submesoscale frontogenesis driven by eddies generates secondary circulations that transport nutrients from depth to the euphotic zone, producing elevated Chl-a concentrations on the warm side of fronts (Zhang et al., 2019). Cyclonic eddies enhance Chl-a through upwelling, whereas anticyclonic eddies suppress it through downwelling (Siegel et al., 2011). Strong dynamical advection within eddy further redistributes nutrients and phytoplankton horizontally (Zhang et al., 2019).

Current researches have systematically examined how ocean eddies interact with temperature fronts and their direct effects on Chl-a concentrations. However, It remains unclear that the regulaion of eddies in the coupling relationship between temperature and Chl-a fronts, as well as their spatiotemporal covariation. To investigate this question, This study focuses on the subarctic frontal zone of the Northwest Pacific (30°N-50°N, 140°E-175°E). Using high-resolution satellite observations of sea surface temperature, Chl-a concentration and surface velocity fields, the lagged cross-correlation analysis is applied to examine the spatiotemporal evolution of temperature and Chl-a fronts under eddy perturbation, together with the time lag inherent in eddy dynamical effects. Furthermore, eddy modulation of the front coupling mechanism will be clarified in this paper The results will provide a scientific basis for understanding the coupled mechanisms between physical fronts and ecological fronts, as well as the oceanic dynamical and biological responses to eddy modulation.

2 Data and Methods

2.1 Data

Three categories of remote satellite observation, sea surface temperature (SST), Chl-a concentration and surface velocity were collected in this study. All data were obtained from the Copernicus Marine Environment Monitoring Service (CMEMS) (https://data.marine.copernicus.eu/product/). Sea surface temperature data were sourced from the Multiscale Ultrahigh Resolution (MUR) Global High-Resolution Sea Surface Temperature (GHRSST) product, with a spatial resolution of 0.01° × 0.01°. Chl-a concentration data were derived from a multi-sensor satellite merged product at 4 km × 4 km resolution. Surface velocity were taken from the Global Ocean Physics Reanalysis, which provides data with the spatial resolution of 0.083° × 0.083°. These daily obsrevations were selected to span from 1 January 2014 to 31 December 2023 and cover the spatial domain 30°N-50°N, 140°E-175°E.

https://doi.org/10.5194/egusphere-2026-4384
Preprint. Discussion started: 4 August 2026

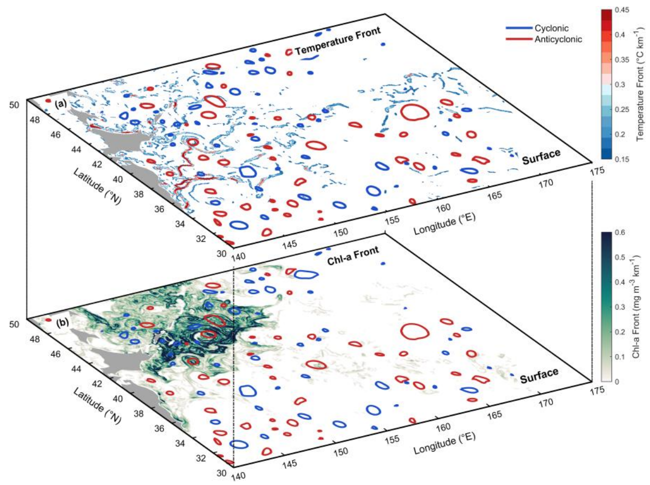

Figure1. Surface fronts and eddy distribution on 26 May 2019.

a, Temperature front. b, Chl-a front. Cyclonic and anticyclonic eddies are outlined in blue and red, respectively.

2.2 Methods

2.2.1 Detection of eddy and front

The identification of mesoscale eddies employed the geometric criterion of Nencioli et al. (Nencioli et al., 2010), which locates eddy centres from the local vector geometry of the two-dimensional velocity field. For each eddy, its boundary was defined as the outermost closed streamline around the centre and calculated its radius as the mean distance from the boundary to the centre. The detection routine ran on daily data and recorded the number of eddies, polarity (cyclonic or anticyclonic), centre coordinates, mean radius, and boundary positions. To separate the eddy interior from the background flow, the interior was taken as within the mean radius and the exterior as the annulus between two and three mean radii. That would reduce the interference from peripheral transitional flows and secondary circulations.

The Sobel algorithm (Sobel and Feldman, 1968) was used to identify temperature and Chl-a fronts based on spatial gradients in oceanographic properties. This method applies convolution kernels to compute weighted sums of the meridional and zonal gradients. Four frontal parameters were usede in this paper. 1) Frontal intensity, defined as the horizontal gradient of sea surface hydrological properties, serves as the primary metric for front detection (Canny, 1986; Vlasenko et al., 2005; McWilliams, 2021). A unified threshold set at the 95th percentile was adopted to detect fronts, drawing on both the traditional gradient method (Canny, 1986; Belkin et al., 2009) and the high-resolution data processing approach (Ping et al., 2014; Xing et al., 2024). This choice can balance noise suppression with the detection of weak fronts and offer greater robustness for identifying persistent fronts (Chu and Wang, 2003; Belkin et al., 2009; Xing et al., 2024; Kim et al., 2025). 2) The front generation probability(FGP) is the likelihood of Chl-a front generation within the eddy's influence after a specific lag period, given that the temperature front already exists while the Chl-a front has not yet emerged. This parameter can be used to quantify the lagged formation of Chl-a fronts by eddies. 3) Front frequency is defined as the probability of front occurrence and is computed as follows (Belkin and O'Reilly, 2009):

$$F = \frac{m}{Days} \times 100\% \tag{1}$$

Where F is the front frequency at a given grid point, m is the number of days when the cell exceeded the 95th-percentile gradient threshold in the current month, and $Days$ is the total days of the month. 4) The fourth parameter,

https://doi.org/10.5194/egusphere-2026-4384
Preprint. Discussion started: 4 August 2026

front frequency ratio (FFR), is the ratio of front frequency in the eddy core (0-1R) to that in the eddy exterior (2-3R). Both are computed in the eddy-centered coordinate system.

2.2.2 Statistical analysis

The spatial correlation between temperature and Chl-a front intensities was quantified by the Pearson correlation coefficient. For a region containing n valid grid cells, the correlation was calculated as

$$r = \frac{\sum_{i=1}^{n}(G_{T,i} - \overline{G_T})(G_{C,i} - \overline{G_C})}{\sqrt{\sum_{i=1}^{n}(G_{T,i} - \overline{G_T})^2 \sum_{i=1}^{n}(G_{C,i} - \overline{G_C})^2}} \quad (2)$$

where G_T and G_C denote the local SST and Chl-a gradient magnitudes, respectively, and the overbar indicates a spatial mean over the region.The two-tailed Student's t-test was permoted (Bjornsson and Venegas, 1997; Wilks, 2011) to validate the correlation analysis. When the p-value was below 0.05, the linear relationship between temperature and Chl-a fronts was considered statistically significant.

The mediation analysis (Preacher and Hayes, 2004) was employed to investigate whether temperature fronts serve as an indirect pathway through which eddies modulate Chl-a fronts. A statistical mediation model was constructed with eddy kinetic energy (EKE) or relative vorticity as the predictor, Chl-a front intensity as the response variable, and temperature front intensity as the mediator. The estimation followed two steps. Firstly, the coefficients were obtained via ordinary least squares regression. One path was temperature front intensity regressed against eddy parameters (path a), and the other was Chl-a front intensity regressed against temperature front intensity (path b). The indirect effect was then quantified as the product of path a and path b, with its 95% confidence interval constructed from 500 Bootstrap resamples. The indirect effect was considered statistically significant when the confidence interval did not contain zero.

3 Results

3.1 Frontal features modulated by eddy

Eddy mixing is expected to produce substantial differences in environmental properties between the eddy core and the exterior, and these differences likely depend on eddy intensity. To quantify this dependence, EKE was classified into five levels (Table 1). For cyclonic (CEs) and anticyclonic (ACEs) eddies separately, the probability density distributions of key environmental variables inside and outside the eddy were compared, and the relationships between ΔSST, ΔChl-a and ΔEKE across intensity levels were examined.

The probability density distribution of SST within CEs is bimodal, with the bulk shifted towards colder water relative to the exterior (Fig. 2 a1). Chl-a exhibits a unimodal pattern both in the eddy core and the exterior. The eddy core has a higher median value and greater dispersion (Fig. 2 b1). The EKE in the eddy core is substantially higher than that of exterior (Fig. 2 c1). All differences are statistically significant ($p < 0.001$ in two-tailed t-test). The EKE difference increases monotonically with EKE magnitude (from −0.03 to 0.11 $m^2\ s^{-2}$). The elevation of core EKE is most prominent in high-EKE CEs (Fig. 2 d1). ΔEKE exhibits weak negative correlations with ΔSST and weak positive correlations with ΔChl-a (Fig. 2 e1-f1). The ΔChl-a values associated with high-EKE are concentrated near the trend line. These features demonstrate the dynamic regulation of CEs in cooling and enhancing productivity.

In contrast, ACEs exhibit warmer SST and lower Chl-a concentrations in the eddy core, with a wider difference in both variables than observed in CEs (Fig. 2 a2-b2). Similar to CEs, the median EKE in eddy core exceeds that of exterior and increases monotonically with eddy intensity. Although the ΔEKE of ACEs is more tightly clustered (Fig. 2 c2-d2). Enhancment of ACEs is associated with the accelerated warming and suppressive Chl-a in the eddy region viewed by the positive correlation of ΔEKE with ΔSST and negative correlation with ΔChl-a. The scatter of all variables in ACEs is more concentrated than CEs. That indicates a stronger dependence of environmental changes on eddy intensity within

https://doi.org/10.5194/egusphere-2026-4384
Preprint. Discussion started: 4 August 2026

ACEs (Fig. 2 e2-f2). These patterns are also evident from Table 1. CEs cool the eddy core and promote Chl-a accumulation, whereas ACEs with warm core suppress Chl-a. For both polarities, more pronounced environmental changes can be easily induced by higher EKE.

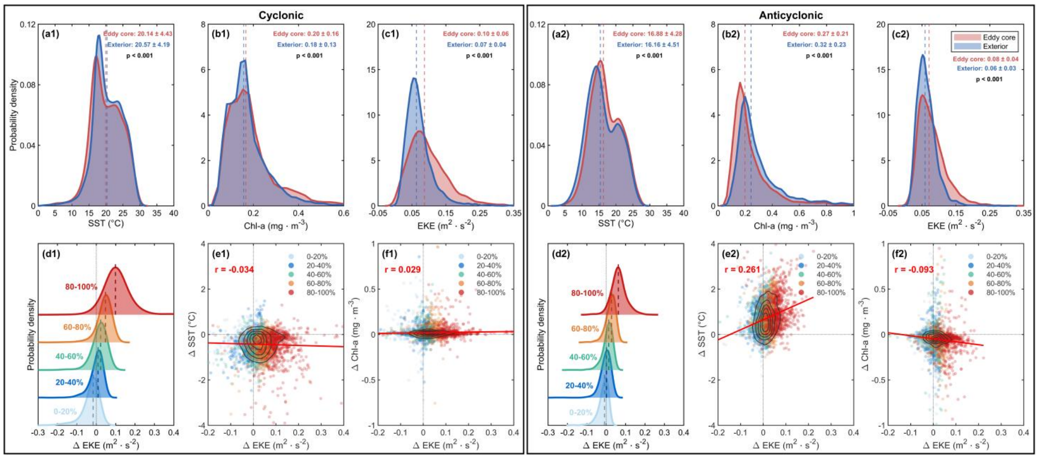

Figure 2. SST, Chl-a, and EKE differences between the eddy core and exterior incuced by eddy.
a-c, Probability density distributions of SST, Chl-a , and EKE in eddy core and exterior. a1-c1 are for CEs. a2-c2 are the same but for ACEs.. d-f, Probability density distributions of ΔEKE and the statistical distribution of ΔEKE with ΔSST and ΔChl-a. d1-f1 are for CEs. d2-f2 are the same but for ACEs..Dashed vertical lines denote the median values; Black dashed lines represent the contours of bivariate probability density. Red lines are linear regressions trend.

Table 1. Mean values of environmental variations in the eddy core and exterior corresponding to differrent EKE levels.

Eddy polarity	EKE level	EKE threshold ($m^2\ s^{-2}$)	n (days)	ΔSST (°C)	ΔChl-a ($mg\ m^{-3}$)	ΔEKE ($m^2\ s^{-2}$)
CEs	Level 1(0-20%)	≤ 0.05	712	-0.320 ± 0.464	0.0120 ± 0.0979	-0.03 ± 0.04
	Level 2(20-40%)	0.05 - 0.07	712	-0.370 ± 0.470	0.0125 ± 0.0663	0.00 ± 0.03
	Level 3(40-60%)	0.07 - 0.10	712	-0.473 ± 0.478	0.0222 ± 0.0607	0.01 ± 0.05
	Level 4(60-80%)	0.10 - 0.14	712	-0.488 ± 0.481	0.0294 ± 0.0905	0.04 ± 0.04
	Level 5(80-100%)	≥ 0.14	712	-0.522 ± 0.699	0.0238 ± 0.0664	0.11 ± 0.07
ACEs	Level 1(0-20%)	≤ 0.05	728	0.524 ± 0.577	-0.0468 ± 0.1592	-0.01 ± 0.03
	Level 2(20-40%)	0.05 - 0.06	728	0.604 ± 0.562	-0.0412 ± 0.1177	0.00 ± 0.03
	Level 3(40-60%)	0.06 - 0.08	727	0.647 ± 0.621	-0.0431 ± 0.1336	0.01 ± 0.03
	Level 4(60-80%)	0.08 - 0.11	728	0.796 ± 0.671	-0.0578 ± 0.1306	0.02 ± 0.03
	Level 5(80-100%)	≥ 0.11	728	1.035 ± 0.782	-0.0725 ± 0.1544	0.06 ± 0.04

The composite in the eddy-centred coordinate system shows that the Chl-a FFR is generally higher than temperature FFR in CEs. The enhancement of Chl-a fronts is more pronounced than that of temperature within eddy regions. The mean Chl-a FFR reaches 1.21 in the eddy core, indicating a preferential occurrence of Chl-a fronts near the eddy centre (Fig. 3a1-b1). The temperature FFR averages approximately 1 in the eddy core, whereas it is elevated (>1) in the peripheral region between 1R and 2R. Both FFRs tend to converge towards equality in this annular zone (Fig. 3d). The EKE composites (Fig. 3c1) show a local minimum (<0.05 $m^2\ s^{-2}$) in the eddy center (within 0.5R), but maintain values of 0.08-0.15 $m^2\ s^{-2}$ in the 1R-2R peripheral band, spatially coincident with the elevated FFR observed in that region.

The FFR distribution in the ACEs region differs markedly from that of CEs (Fig. 3a2-b2). The temperature FFR

https://doi.org/10.5194/egusphere-2026-4384
Preprint. Discussion started: 4 August 2026

averages only 0.28 in the eddy core and reaches 1.0 in the exterior. In other words, the probability of temperature front occurrence near the eddy centre is less than one-third of that in the exterior. The Chl-a FFR in the core has a mean value of 0.74, also suppressed by the anticyclonic eddy but to a lesser degree than the temperature FFR. Outside the 1.5R radius in the northern sector, the ACEs enhance temperature and Chl-a FFR (FFR > 1). Correspondingly, the elevated EKE of ACEs is also concentrated beyond the mean radius and is shifted northward overall (Fig. 3c2).

The radial curves in Fig. 3d show that Chl-a FFR consistently exceeds temperature FFR within CEs and its enhancement over the background decreases monotonically with radial distance. Temperature FFR, by contrast, first increases and then decreases with radius. Both FFRs remain above unity and overlap spatially between 0.5R and 1.5R. For ACEs, the FFR distribution exhibits a characteristic interior minimum and exterior maximum, increasing monotonically from the core outward. Chl-a FFR is less sensitive than temperature FFR to the suppressive effect of ACEs. In both eddy polarities, the perturbation to front frequency diminishes substantially outside the eddy. Where FFR approaches unity and the standard deviation increases monotonically with radial distance, indicating that the ambient frontal field outside the eddy is not statistically stable.

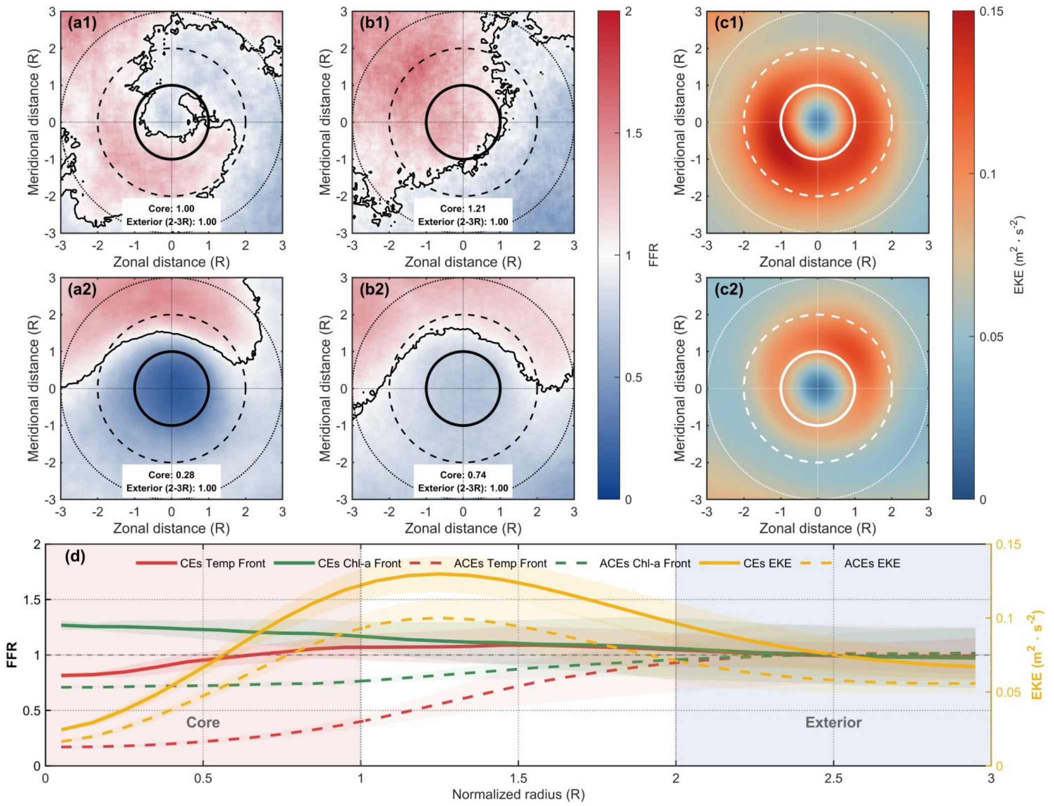

Figure3. Spatial distribution of fronts in the eddy-centred coordinate system.

a1-c1, Meridional composites of temperature FFR, Chl-a FFR, and EKE within CEs. a2-c2, Same as a1-c1, but for ACEs. d, Curves of temperature FFR, Chl-a FFR, and EKE from the eddy core to the exterior. Solid circles mark the mean eddy radius. Dashed circles indicate eddy boundaries at 2R and 3R. The black contours are FFR=1, with FFR>1 denoting frontal enhancement and FFR<1 indicating suppression.

https://doi.org/10.5194/egusphere-2026-4384
Preprint. Discussion started: 4 August 2026

3.2 Frontal coupling under eddy regulation

As shown in Sect. 3.1, when both fronts co-occur in eddy regions, Chl-a fronts are predominantly found within the interiors of CEs and at the peripheries of ACEs, whereas temperature fronts are most likely to occur at the boundaries of both CEs and ACEs. That represents two distinct mechanisms of eddy-induced frontal perturbation: 1) eddies actively promote the generation of new fronts through frontogenesis associated with mesoscale straining (Lu and Kamenkovich, 2025); 2) eddies stir surrounding pre-existing frontal structures into their interiors through eddy stirring without generating new fronts themselves (Naveira Garabato et al., 2011).

To clarify the promoting role of eddy, Fig. 4 presents the FGP of Chl-a fronts within 21 days following the co-occurrence of temperature fronts and eddies. Within the eddy core of CEs, the FGP of Chl-a induced by temperature fronts is substantially higher than exterior. A similar but weaker enhancement is displayed for ACEs (Fig. 4 a-b). For CEs, higher EKE levels correspond to higher FGP, indicating that CEs intensity promotes frontal coupling. ACEs also exhibit a notable promoting effect, although this dynamical influence is inversely related to ACEs intensity. At low EKE level (Level 1), however, the frontal coupling shows some randomness with respect to eddy intensity. The lagged FGP of Chl-a across EKE levels shows a tendency to first increase and then decrease in the CEs region. The peaks occurr at lags of 3-8 days and most values falling below 1% after 21 days. As for ACEs, the lagged FGP varies more smoothly, with two intervals of elevated generation likelihood at 3-5 days and 13-18 days after the temperature front appears.

The differences in lagged FGP between CEs and ACEs (Fig. 4 c) declare that at low or moderate eddy intensities (Level 1-Level 3), the two eddy types contribute comparably to frontal coupling within the first 10 lag days, with CEs showing a slight advantage. After 12 days, ACEs exhibit a significantly greater regulatory advantage. When the EKE level is higher (>Level 3), the FGP difference at a 7-day lag reaches 5.1%. Overall, the promoting effect of CEs on frontal coupling is concentrated in the short-term lag phase (approximately 3-8 days), whereas that of ACEs is manifested in longer-term regulation.

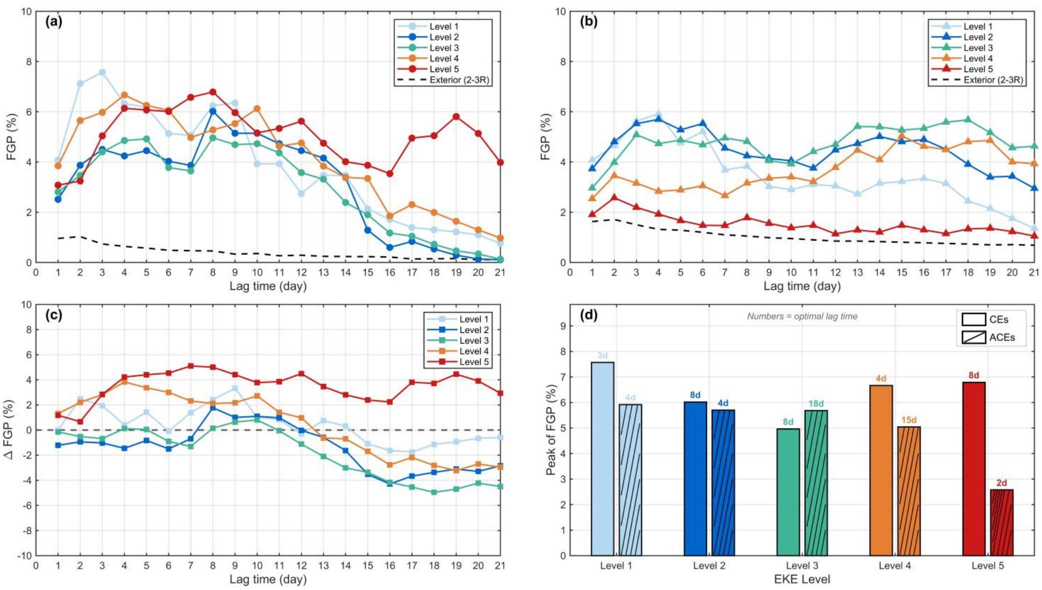

Figure4. FGP of Chl-a induced by temperature fronts in the presence of eddies.
a, Lagged FGP of Chl-a induced by temperature ronts corresponding to each EKE level and eddy exterior in CEs. b, The same as a, but for ACEs. c, Difference in FGP of Chl-a between CEs and ACEs . d, Statistic of FGP peak and corresponding optimal lag days for each EKE level.

https://doi.org/10.5194/egusphere-2026-4384
Preprint. Discussion started: 4 August 2026

Figure 5 further examines the lagged correlation between temperature fronts and Chl-a fronts under eddy-induced dynamical perturbations. Overall, the sample size for frontal coupling within CEs decreases markedly after a lag of one week, consistent with the short-term regulatory effect of CEs (Fig. 4). In contrast, ACEs exhibit a longer duration in frontal coupling and more pronounced coupling features, as reflected in higher correlations between the two frontal intensities. In the CEs region (Fig. 5 a1-b1), temperature front intensity and Chl-a front intensity show a significant positive correlation ($p < 0.05$) at lags of 0-2 days, meaning that the two fronts vary in the same direction. With the lag time getting longer, the correlation turns negative. The transition occurrs at lags of 3-6 days depending on eddy intensity. Within ACEs, at lower eddy intensity (Level 2), the two fronts show a significant positive correlation for seven consecutive days (Fig. 5 a2-b2). Corresponding to the higher eddy intensities, the positive coupling between the two fronts persists for about 3 days, after which positive and negative correlations alternate. Both frontal intensities are mostly negatively correlated when the lag time reaches 10 days or more.

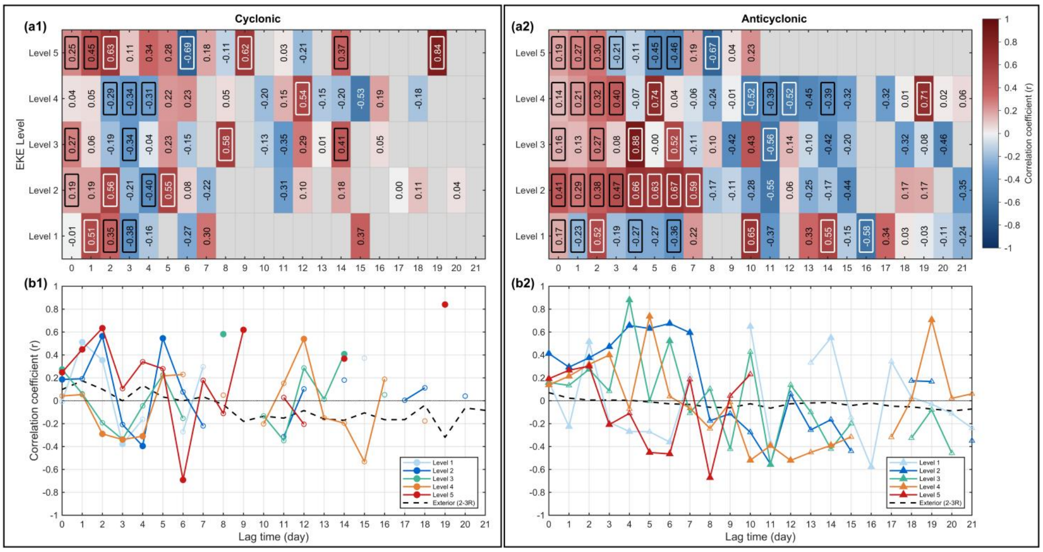

Figure 5. Lagged correlation of forntal coupling of temperature front and Chl-a front within eddies.
a1-a2, Heatmaps of lagged correlation coefficients of temperature front intensity and Chl-a front intensity in CEs (a1) and ACEs (a2) . b1-b2, Lagged orrelation coefficients for different EKE level and exterior in CEs (b1) and ACEs(b2) . The boxed values indicate statistical significance at the $p < 0.05$ level; grey grids denote insufficient sample sizes. Solid markers denote statistical significance ($p < 0.05$), whereas open markers indicate non-significance.

3.3 Impact of eddy evolution on frontal coupling

During the evolution of eddies from generation to dissipation, the frontal coupling characteristics within the eddy region undergo continuous changes due to the energy accumulation and dissipation. The eddy life cycle is divided into formation (0-10%), intensification (10-30%), mature (30-80%), and decay (80-100%) in this section (Liu et al., 2012; Gaube et al., 2014). Figures 6 and 7 present the influence of eddy evolution on the front frequency within CEs and ACEs, respectively.

The relative vorticity of CEs exhibits a typical quadrupole structure (Fig. 6a). The spatial distribution, positive vorticity in the upper-left and negative vorticity in the upper-right, is a signature of anticlockwise rotating flow under a deformation field.. During the formation stage when the eddy separates from background flow instability, negative vorticity dominates the eddy core (Fig. 6 a1). The temperature front frequency shows a broad high-value region on the

https://doi.org/10.5194/egusphere-2026-4384
Preprint. Discussion started: 4 August 2026

western side of the eddy, most pronounced in the southwest (Fig. 6 b1). While the Chl-a front frequency is elevated on the northwest side and generally lower than temperature front frequency (Fig. 6 c1). In the intensification stage (Fig. 6 a2), the absolute vorticity increases and the negative vorticity core contracts notably, accompanied by a concurrent contraction of both temperature and Chl-a front frequencies (Fig. 6 b2, c2). Eddies reach a quasi-geostrophic balance in the mature stage. The relative vorticity becomes more axisymmetric and frontal coupling is mostly concentrated at the eddy periphery (between 1R and 2R) (Fig. 6 a3, b3, c3). As the eddy energy dissipates (Fig. 6 a4), relative vorticity weakens and the symmetric structure becomes less stable. Although the eddy core maintains a positive vorticity advantage. Both frontal frequencies recover slightly, occurring more frequently in the exterior and gradually merging into the background (Fig. 6 b4, c4).

During the formation and intensification stages, the interaction between the eddy and the background flow is most vigorous. The eddy periphery is highly unstable and thus frequently generate both temperature and Chl-a fronts. The temperature front frequency shows a tendency to first increase and then decrease from eddy core to exterior and Chl-a frequency has a decreasing pattern. These characteristics are most pronounced at the formation stage and diminish gradually as the eddy evolves (Fig. 6d). Within the eddy core, temperature and Chl-a front frequencies exhibit opposite trends, whereas in the eddy exterior, their trends become aligned.

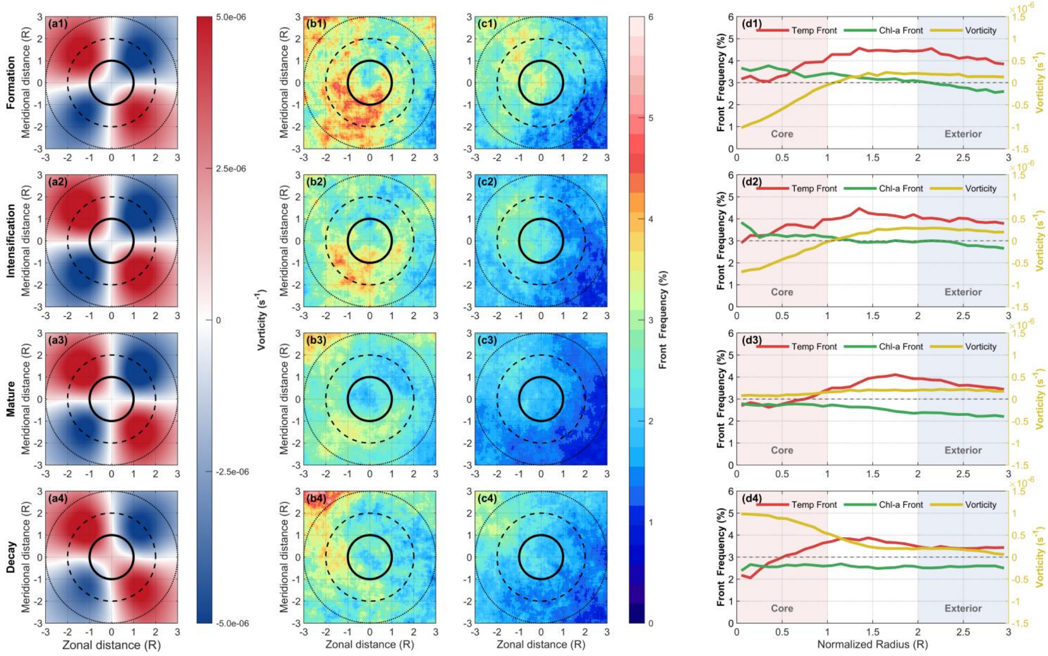

Figure 6. Spatial distribution and radial evolution of front frequency and relative vorticity across the lifecycle of cyclonic eddies. a1-a4, Composite of relative vorticity corresponding to formation, intensification, mature, and decay of CEs. b1-b4, Same as a1-a4 but for temperature front frequency. c1-c4, Same as a1-a4 but for Chl-a front frequency. d1-d4, Radial evolution for front frequency and relative vorticity within CEs. The black solid and dashed lines denote 1R, 2R, and 3R radii, respectively. The grey dashed line represents the zero contour of relative vorticity.

ACEs also exhibit a quadrupole structure, but with reversed polarity: positive in the upper-right and negative in the upper-left. It's a signature of clockwise rotating flow (Fig. 7a). From formation to mature, the eddy's rotation speed increases and the negative vorticity in the core region gradually intensifies. High values of temperature and Chl-a front frequency co-occur on the northern and exterior of the eddy. Moreover, both front frequencies show a synchronous

https://doi.org/10.5194/egusphere-2026-4384
Preprint. Discussion started: 4 August 2026

reduction with the evolution of ACEs. This indicates a strong front coupling characteristics. In comparison, the Chl-a front frequency is lower than that of temperature. During the decay stage of ACEs (Fig. 7a4), the core negative vorticity weakens significantly and approaches a symmetric distribution. Meanwhile, the frequencies of these two fronts experience a further reduction. Throughout the entire evolution of theACEs, the front frequency in the eddy core remains at extremely low levels. Although the difference in temperature front frequency between the interior and exterior of ACEs is more pronounced than that of the Chl-a front, the variation patterns of both are relatively consistent (Fig. 7d). This further reflects the dynamic suppression of frontogenesis by the internal circulation of ACEs. Meanwhile, it implies that ACEs can enhance front coupling in their exterior regions.

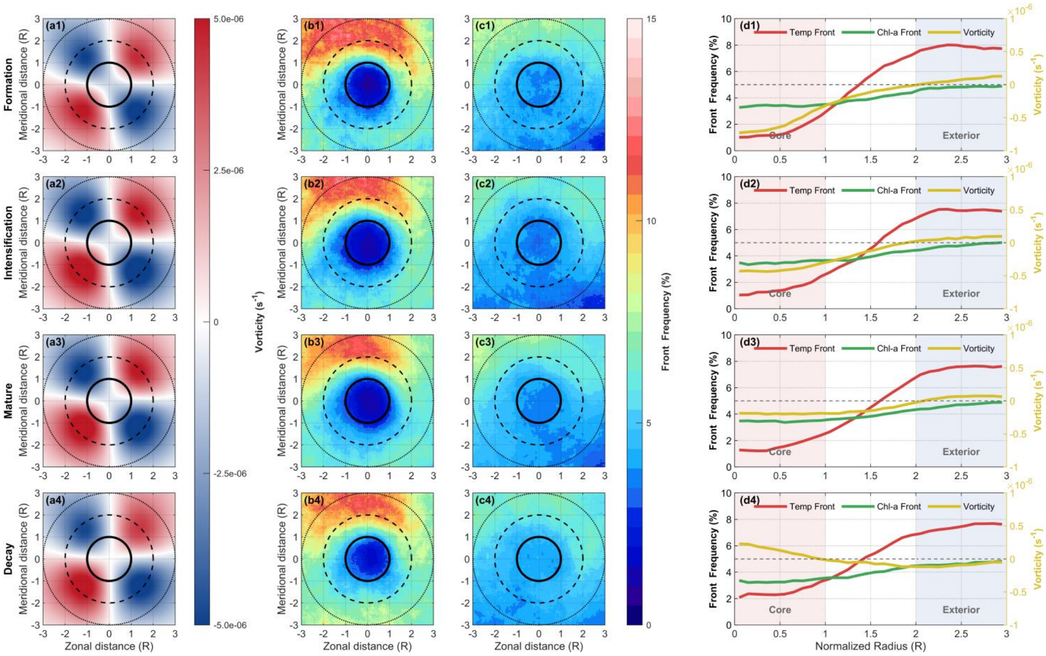

Figure 7. Same as Figure 6, but for ACEs.

a1-a4, Composite of relative vorticity corresponding to formation, intensification, mature, and decay of ACEs. b1-b4, Same as a1-a4 but for temperature front frequency.c1-c4, Same as a1-a4 but for Chl-a front frequency. d1-d4, Radial evolution for front frequency and relative vorticity within ACEs. The black solid and dashed lines denote 1R, 2R, and 3R radii, respectively. The grey dashed line represents the zero contour of relative vorticity.

4 Discussion

4.1 Differences in eddy regulation of the two Fronts

Eddies can modulate frontal intensity through straining and convergence processes (Wu and Jing, 2026), yet this modulation exhibits both interrelated and distinctly different spatiotemporal responses between temperature fronts and Chl-a fronts. As shown in Fig. 8, within the eddy core of CEs, temperature front intensity remains relatively low from lag day 0 to day 9, then increases rapidly and reaches a peak of 0.43°C km^{-1} at lag day 16. For ACEs, the temporal fluctuation is generally weaker than that of CEs, with the core temperature front intensity reaching a minimum of 0.21°C km^{-1} at lag day 8 before rising again to a peak of 0.36°C km^{-1} at lag day 16. The optimal enhancement window for both

https://doi.org/10.5194/egusphere-2026-4384
Preprint. Discussion started: 4 August 2026

eddy types occurs around lag day 16, suggesting that this timescale may reflect an intrinsic period of energy conversion from eddies to frontal gradients, independent of eddy polarity.

The lagged response of Chl-a front intensity is distinctly different from that of temperature fronts (Fig. 8b). Within the eddy core of CEs, Chl-a front intensity reaches a peak of 0.54 mg m⁻³ km⁻¹ at lag day 1, then decreases continuously to a minimum of 0.06 mg m⁻³ km⁻¹ at lag day 9, showing an overall declining trend. ACEs exhibit a similar declining trend but with a relatively milder amplitude. The difference curves (Fig. 8d) reveal that the negative difference in Chl-a front intensity between the eddy core and the exterior (core < exterior) lasts longer and is greater in magnitude (minimum of −0.46 mg m⁻³ km⁻¹) for CEs than for ACEs.

The temporal responses of temperature fronts and Chl-a fronts are asynchronous. The optimal enhancement window for temperature fronts occurs around lag day 16, whereas Chl-a fronts show a phased response characterized by early enhancement, mid-term suppression, and late recovery. This asynchrony may reflect an inherent time lag in the physical-biological coupling process: eddies first modulate temperature fronts through dynamical processes (physical response), and then indirectly affect Chl-a fronts through nutrient supply and changes in the light environment (biological response), with a time lag of several days to more than ten days between the two.

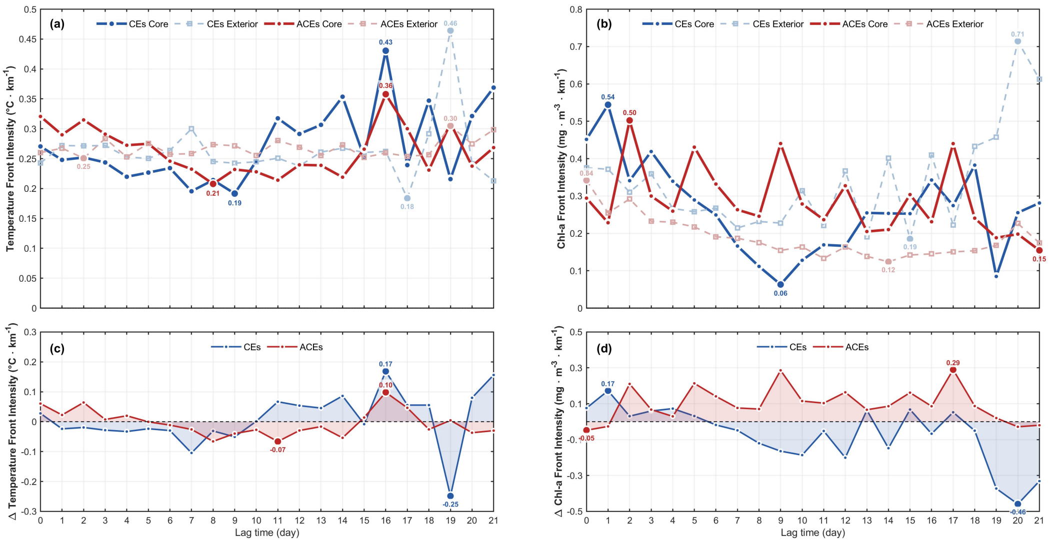

Figure 8. The lagged response of frontal intensity for eddy.

a-b, Lagged time series of temperature front intensity and Chl-a front intensity within the eddy core and exterior region. c-d, Lagged time series of the core-exterior differences in the front intensity for temperature and Chl-a .Blue lines denote CEs and red lines denote ACEs.

The modulation of fronts by eddies depends not only on time lag, but also on the developmental stage and spatial extent of the eddies. Spatially, temperature front intensity is higher outside than inside the eddy core for both CEs and ACEs (Fig. 9a), suggesting a possible frontal convergence effect in the exterior region. Temporally, within the eddy core of CEs, temperature front intensity reaches its maximum during the intensification stage, followed by the formation stage, indicating that the developmental stage exerts a strong promoting effect on temperature fronts. For ACEs, temperature front intensity in the core is relatively higher during the decay stage, whereas at the 3R boundary, the differences among life stages are minor. Chl-a front intensity in the eddy core is higher than in the exterior for CEs, whereas the opposite is true for ACEs (Fig. 9b). Moreover, the variation in Chl-a front intensity across different life stages is substantially larger

https://doi.org/10.5194/egusphere-2026-4384
Preprint. Discussion started: 4 August 2026

for CEs than for ACEs, suggesting that the modulation of biological variables by eddies is more sensitive to life-cycle evolution in CEs.

In summary, the modulation of temperature and Chl-a fronts by eddies exhibits distinct spatiotemporal patterns. Temporally, the lag between the responses of the two frontal types reflects the inherent time delay in physical-biological coupling. Spatially, the eddy core is the primary region of frontal enhancement, with modulation intensity varying significantly across life stages-strongest during the formation and intensification stages and weakest during the decay stage.

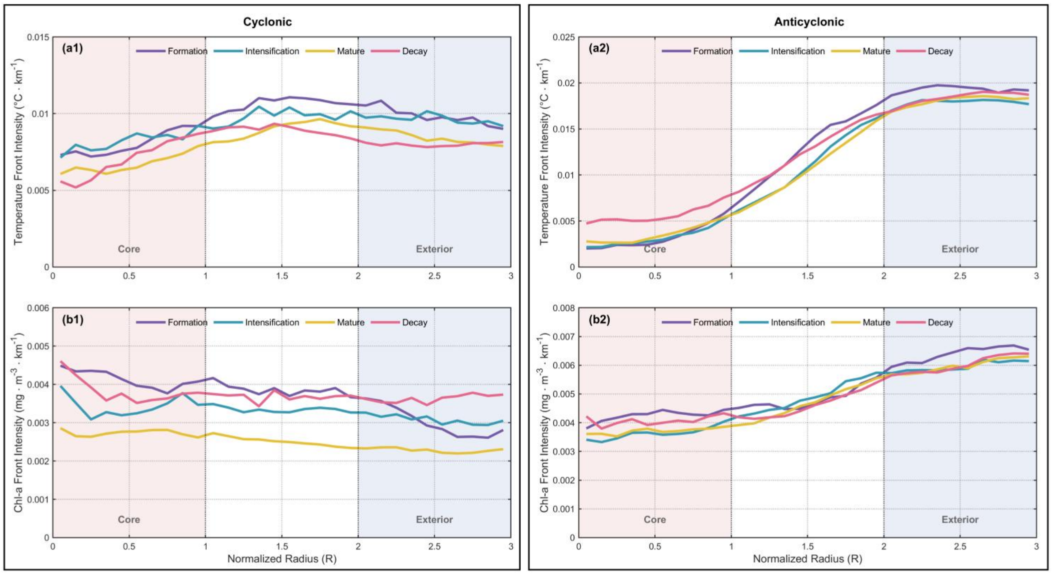

Figure 9. Radial distribution of frontal intensity across different lifecycle stages within CEs and ACEs.
a1-a2, Radial variation of temperature front intensity for CEs and ACEs, stratified by lifecycle stage. b1-b2, Same as a1-a2 but for Chl-a front intensity.

4.2 Mediating mechanism of the temperature front

As mentioned above, the frontal coupling modulated by eddy exhibits a certain lag time and temperature front plays a crucial mediating role. Detailed mediation coefficients for all lag days, including path coefficients a, b, total effect c, indirect effect a×b, and their 95% bootstrap confidence intervals, are provided in Appendix Tables A1–A4. Mediation analysis within the eddy core of CEs reveals that both pathways are dominated by significant negative mediation ($a \times b < 0$) (Table 2), although the specific mechanisms vary with lag time. The significant negative mediation occurs at lags of 0, 1, 3, 4 and 19 days along the regression pathway modulated by EKE (Model 1). At lags of 0, 1 and 19 days, increased EKE is associated with weakened temperature fronts ($a < 0$), and weakened temperature fronts limit Chl-a front enhancement ($b > 0$). Thus, EKE indirectly suppresses Chl-a fronts by weakening temperature fronts. At lags of 3 and 4 days, increased EKE is associated with strengthened temperature fronts ($a > 0$), but enhanced temperature fronts are detrimental to Chl-a front maintenance ($b < 0$). EKE indirectly suppresses Chl-a fronts by strengthening temperature fronts. This pathway exhibits the strongest effect at lag 19 days ($c = -0.6145$, $a \times b = -0.3327$, contribution rate: 54.1%). As for the relative vorticity (Model 2), there are the similar mediating mechanism of the temperature front. The corresponding lag time varies slightly, accompanied by a decrease in significance.

In ACEs, the significant mediating effects in Model 1 are predominantly positive. At lags of 0-7 and 9 days, increased EKE strengthens temperature fronts ($a > 0$), which in turn promote Chl-a fronts ($b > 0$). At lags of 7 days, the

https://doi.org/10.5194/egusphere-2026-4384
Preprint. Discussion started: 4 August 2026

total effect indicates that temperature fronts offsetting the suppressive effect of EKE on Chl-a fronts. At lags of 11, 13-15 and 20 days, increased EKE weakens temperature fronts ($a < 0$), and weakened temperature fronts suppress Chl-a fronts ($b < 0$). In this case, temperature fronts act as a suppressive mediator, but this suppression is weakened by EKE, thereby reducing the overall suppression on Chl-a fronts and indirectly promoting them. However, the contribution rate at the optimal lag (7 days) is negative (−88.1%), indicating that although the temperature front pathway promotes Chl-a fronts. In Model 2, the significant mediating effects are negative at lags of 1-4 days: increased relative vorticity weakens temperature fronts, which in turn weaken Chl-a fronts ($a < 0$, $b > 0$). The optimal lag effect at 16 days is not statistically significant (confidence interval crossing zero). Overall, the significant mediating effects in ACEs are mostly confined to within 10 days, and the effect intensity is generally weaker than that in CEs.

https://doi.org/10.5194/egusphere-2026-4384
Preprint. Discussion started: 4 August 2026

Table 2. Comparison of lagged   lagged responses to the mediating effects of temperature fronts between CEs and ACEs.

Lag time (day)	CEs				ACEs			
	Model 1 (EKE→Temp→Chl-a)		Model 2 (Vort→Temp→Chl-a)		Model 1 (EKE→Temp→Chl-a)		Model 2 (Vort→Temp→Chl-a)	
	$a \times b$	95% CI	$a \times b$	95% CI	$a \times b$	95% CI	$a \times b$	95% CI
0	**-0.0226**	[-0.0404, -0.0098]	0.0056	[-0.0082, 0.0188]	**0.0260**	[0.0145, 0.0413]	-0.0082	[-0.0197, 0.0012]
1	**-0.0348**	[-0.0599, -0.0148]	0.0116	[-0.0124, 0.0428]	**0.0229**	[0.0078, 0.0428]	**-0.0137**	[-0.0265, -0.0023]
2	-0.0005	[-0.0242, 0.0150]	-0.0165	[-0.0557, 0.0062]	**0.0323**	[0.0025, 0.0634]	**-0.0645**	[-0.0959, -0.0365]
3	**-0.0707**	[-0.1467, -0.0286]	-0.0358	[-0.0869, 0.0177]	**0.0587**	[0.0193, 0.1138]	**-0.0496**	[-0.0921, -0.0190]
4	**-0.0497**	[-0.0880, -0.0205]	**-0.0697**	[-0.1365, -0.0104]	**0.0951**	[0.0395, 0.1681]	**-0.0418**	[-0.1000, -0.0035]
5	0.0291	[-0.0224, 0.1678]	-0.0024	[-0.0277, 0.0169]	**0.0899**	[0.0182, 0.1929]	-0.0022	[-0.0394, 0.0311]
6	0.0040	[-0.0254, 0.0388]	-0.0024	[-0.0253, 0.0152]	**0.0965**	[0.0065, 0.2149]	0.0021	[-0.0336, 0.0471]
7	-0.0141	[-0.1071, 0.0580]	-0.0309	[-0.1447, 0.0265]	**0.2150**	[0.1128, 0.3489]	0.0115	[-0.0027, 0.0344]
8	-0.0143	[-0.0489, 0.0271]	-0.0070	[-0.0333, 0.0240]	-0.0151	[-0.0584, 0.0259]	0.0133	[-0.0219, 0.0475]
9	-0.0832	[-0.2506, 0.0077]	0.1574	[-0.0360, 0.3287]	**0.1884**	[0.0100, 0.4551]	0.0559	[-0.0275, 0.1691]
10	-0.0250	[-0.1015, 0.0348]	-0.0074	[-0.0616, 0.0272]	-0.0834	[-0.2546, 0.0878]	-0.0240	[-0.0796, 0.0188]
11	0.0095	[-0.0305, 0.0593]	**0.0949**	[0.0112, 0.1776]	**0.1157**	[0.0604, 0.2512]	0.0291	[-0.0360, 0.0979]
12	-0.0421	[-0.1032, 0.0010]	-0.0129	[-0.0924, 0.0475]	0.0161	[-0.0249, 0.0646]	0.0062	[-0.0395, 0.0416]

https://doi.org/10.5194/egusphere-2026-4384
Preprint. Discussion started: 4 August 2026

Lag time (day)	CEs				ACEs			
	Model 1 (EKE→Temp→Chl-a)		Model 2 (Vort→Temp→Chl-a)		Model 1 (EKE→Temp→Chl-a)		Model 2 (Vort→Temp→Chl-a)	
	a × *b*	95% CI	*a* × *b*	95% CI	*a* × *b*	95% CI	*a* × *b*	95% CI
13	-0.0034	[-0.0670, 0.1065]	0.0179	[-0.0185, 0.1348]	**0.0376**	[0.0062, 0.0805]	**0.0586**	[0.0100, 0.1379]
14	-0.0540	[-0.1078, 0.0013]	-0.0230	[-0.1236, 0.0859]	**0.0547**	[0.0106, 0.1189]	-0.0025	[-0.0560, 0.0362]
15	-0.0052	[-0.1494, 0.0537]	-0.0510	[-0.2340, 0.0620]	**0.1059**	[0.0138, 0.2196]	-0.0223	[-0.0761, 0.0118]
16	0.0473	[-0.0691, 0.2382]	-0.0033	[-0.0467, 0.0783]	0.1124	[-0.0669, 0.3370]	-0.0717	[-0.3692, 0.1976]
17	0.0454	[-0.0005, 0.1033]	-0.1283	[-0.3526, 0.0089]	0.0783	[-0.0668, 0.2627]	0.0098	[-0.0537, 0.1161]
18	-0.1010	[-0.4338, 0.1241]	0.0034	[-0.0755, 0.0772]	0.0056	[-0.0463, 0.0425]	-0.0078	[-0.0510, 0.0240]
19	**-0.3327**	[-0.6144, -0.1014]	**-0.3022**	[-0.7667, -0.0982]	**-0.0508**	[-0.1180, -0.0014]	-0.0043	[-0.0363, 0.0348]
20	0.0033	[-0.0529, 0.0905]	0.0598	[-0.0873, 0.1816]	**0.0799**	[0.0069, 0.2310]	-0.0276	[-0.1082, 0.0161]
21	—	—	—	—	-0.0043	[-0.0440, 0.0052]	0.0027	[-0.0074, 0.0165]

345 Note: Results are based on the eddy core region (0-1R), including both cyclonic and anticyclonic eddies. The table presents the indirect effects (a × b) and contribution rates (%) of temperature fronts between EKE (Model 1) or relative vorticity (Model 2) and Chl-a fronts, with lag days ranging from 0 to 21. Values in square brackets denote the Bootstrap 95% confidence interval. Bold values indicate significant indirect effects (95% confidence interval not crossing zero). Data for Lag 21 in cyclonic eddies are missing due to insufficient sample size and are denoted by "—".

https://doi.org/10.5194/egusphere-2026-4384
Preprint. Discussion started: 4 August 2026

5 Data availability

The remote-sensing data used in this study are available from the Copernicus Marine Environment Monitoring Service (CMEMS, https://data.marine.copernicus.eu/). Sea surface temperature data were sourced from the Multiscale Ultrahigh Resolution (MUR) Global High-Resolution Sea Surface Temperature (GHRSST) product, available under the following DOI: https://doi.org/10.48670/moi-00169 (JPL MUR MEaSUREs Project, 2022). Chl-a concentration data were derived from the Global Ocean Colour (Copernicus-GlobColour) Bio-Geo-Chemical, L4 (daily) from Satellite Observations, available under the following DOI: https://doi.org/10.48670/moi-00281 (CMEMS, 2024). Surface velocity data were taken from the Global Ocean Physics Reanalysis (GLORYS12V1), available under the following DOI: https://doi.org/10.48670/moi-00021 (Lellouche et al., 2021).

6 Conclusions

The spatial distribution patterns of temperature and Chl-a fronts vary significantly depending on the regulating of CEs and ACEs. CEs enhance Chl-a fronts in the eddy core and concentrate temperature fronts in the transition zone, whereas ACEs suppress both frontal types in the core with recovery in the periphery. The FFR of Chl-a fronts is consistently higher than that of temperature fronts in both eddy types, with a phase shift in their radial distributions. Moreover, the spatial decay of EKE corresponds spatially to the radial variations in frontal frequency ratio.

Eddies exert a significant modulation on the frontal coupling, although the timescales of regulation effect differ markedly between CEs and ACEs. The FGP of Chl-a fronts induced by temperature fronts is substantially higher in the eddy core than in the exterior within CEs. and increases with eddy intensity. The highest frequency occurs 3-8 days after the temperature front. This indicates that CEs promote the frontal coupling with stronger eddy intensity leading to stronger coupling. ACEs also exhibit frontal coupling, which is inversely related to eddy intensity. The lag time is mostly greater than 10 days. The enhancing effect of eddies on frontal coupling is mostly confined to within one week of lag. Beyond this period, the coupling probability decays more rapidly in CEs and ACEs.

Frontal coupling depends on eddy polarity and evolution stage. Front frequencies are significantly enhanced in the core and peripheral regions during the formation and intensification stages of CEs. Temperature and Chl-a fronts show opposite trend within the eddy core but converging outside. Within ACEs, front frequencies remain extremely low in the core throughout the life cycle. And the frontal coupling occurrs primarily in the exterior (2R-3R) where the two frontal types exhibit broadly consistent spatiotemporal patterns.

The responses of temperature and Chl-a fronts to eddy forcing are distinctly asynchronous. The optimal enhancement of temperature fronts occurs around lag day 16, whereas Chl-a fronts exhibit a phased response characterised by early enhancement, mid-term suppression and late recovery. This asynchrony reflects the inherent time lag in physical-biological coupling: eddies first modulate temperature fronts through dynamical processes (physical response), and then indirectly affect Chl-a fronts through nutrient supply and changes in the light environment (biological response), with a time lag of several days to more than ten days between the two.

https://doi.org/10.5194/egusphere-2026-4384
Preprint. Discussion started: 4 August 2026

Appendix A

Table A1. Mediating effects of EKE on Chl-a via temperature fronts within the eddy core (0-1R) of CEs

Lag time (day)	a	95% CI	b	95% CI	c	95% CI	a×b	95% CI	Contribution rates(%)
0	**-0.1512**	[-0.2321, -0.0704]	**0.1496**	[0.0690, 0.2302]	**-0.1752**	[-0.2557, -0.0947]	**-0.0226**	[-0.0404, -0.0098]	12.9
1	**-0.1602**	[-0.2719, -0.0484]	**0.2171**	[0.1067, 0.3276]	**-0.1734**	[-0.2849, -0.0619]	**-0.0348**	[-0.0599, -0.0148]	20.1
2	-0.0054	[-0.1459, 0.1351]	0.0983	[-0.0410, 0.2375]	-0.1148	[-0.2544, 0.0248]	-0.0005	[-0.0242, 0.0150]	0.5
3	**0.2170**	[0.0799, 0.3542]	**-0.3257**	[-0.4599, -0.1915]	**-0.1848**	[-0.3228, -0.0467]	**-0.0707**	[-0.1467, -0.0286]	38.3
4	**0.2225**	[0.0668, 0.3782]	**-0.2233**	[-0.3780, -0.0685]	**-0.2574**	[-0.4117, -0.1031]	**-0.0497**	[-0.0880, -0.0205]	19.3
5	**0.3497**	[0.1693, 0.5301]	0.0832	[-0.1120, 0.2785]	**-0.3160**	[-0.4987, -0.1333]	0.0291	[-0.0224, 0.1678]	-9.2
6	**-0.1948**	[-0.3643, -0.0253]	-0.0207	[-0.1923, 0.1509]	**-0.2428**	[-0.4104, -0.0751]	0.0040	[-0.0254, 0.0388]	-1.7
7	**0.3305**	[0.0929, 0.5681]	-0.0428	[-0.2421, 0.1565]	**0.6704**	[0.4836, 0.8572]	-0.0141	[-0.1071, 0.0580]	-2.1
8	**0.3205**	[0.0820, 0.5590]	-0.0445	[-0.3077, 0.2186]	-0.1850	[-0.4324, 0.0625]	-0.0143	[-0.0489, 0.0271]	7.7
9	**0.4912**	[0.1473, 0.8352]	-0.1693	[-0.5804, 0.2418]	**-0.4349**	[-0.7905, -0.0794]	-0.0832	[-0.2506, 0.0077]	19.1
10	0.2243	[-0.0555, 0.5041]	-0.1113	[-0.4070, 0.1845]	-0.0444	[-0.3312, 0.2424]	-0.0250	[-0.1015, 0.0348]	56.2
11	**-0.2484**	[-0.4744, -0.0225]	-0.0384	[-0.2469, 0.1701]	**-0.5096**	[-0.7103, -0.3089]	0.0095	[-0.0305, 0.0593]	-1.9

https://doi.org/10.5194/egusphere-2026-4384
Preprint. Discussion started: 4 August 2026

12	-0.2019	[-0.4070, 0.0032]	**0.2083**	[0.0067, 0.4099]	**-0.2822**	[-0.4831, -0.0812]	-0.0421	[-0.1032, 0.0010]	14.9
13	0.2016	[-0.0558, 0.4591]	-0.0170	[-0.2730, 0.2389]	**-0.3261**	[-0.5746, -0.0777]	-0.0034	[-0.0670, 0.1065]	1.1
14	**-0.2626**	[-0.4561, -0.0692]	**0.2058**	[0.0120, 0.3995]	**-0.3162**	[-0.5064, -0.1260]	-0.0540	[-0.1078, 0.0013]	17.1
15	0.0502	[-0.3157, 0.4160]	-0.1038	[-0.4172, 0.2097]	**0.5332**	[0.2233, 0.8431]	-0.0052	[-0.1494, 0.0537]	-1.0
16	**0.4216**	[0.1494, 0.6939]	0.1121	[-0.2163, 0.4405]	0.1707	[-0.1251, 0.4666]	0.0473	[-0.0691, 0.2382]	27.7
17	-0.3739	[-0.7739, 0.0262]	-0.1213	[-0.3867, 0.1441]	**0.8230**	[0.5780, 1.0680]	0.0454	[-0.0005, 0.1033]	5.5
18	0.6591	[0.4408, 0.8773]	-0.1532	[-0.5350, 0.2286]	-0.1713	[-0.4572, 0.1146]	-0.1010	[-0.4338, 0.1241]	58.9
19	**-0.5000**	[-0.8648, -0.1351]	**0.6655**	[0.3972, 0.9338]	**-0.6145**	[-0.9469, -0.2822]	**-0.3327**	[-0.6144, -0.1014]	54.1
20	-0.0591	[-0.5247, 0.4065]	-0.0561	[-0.4116, 0.2993]	**0.6715**	[0.3258, 1.0171]	0.0033	[-0.0529, 0.0905]	0.5
21	—	—	—	—	—	—	—	—	—

Note: Bold values indicate significant indirect effects (95% CI not crossing zero). Data for Lag 21 are not shown due to insufficient sample size.

Table A2. Mediating effects of relative vorticity on Chl-a via temperature fronts within the eddy core (0-1R) of CEs

Lag time (day)	a	95% CI	b	95% CI	c	95% CI	a×b	95% CI	Contribution rates(%)
0	0.0325	[-0.0492, 0.1143]	**0.1708**	[0.0903, 0.2513]	0.0627	[-0.0189, 0.1443]	0.0056	[-0.0082, 0.0188]	8.9
1	0.0497	[-0.0634, 0.1628]	**0.2333**	[0.1239, 0.3427]	**0.1335**	[0.0212, 0.2457]	0.0116	[-0.0124, 0.0428]	8.7
2	-0.1335	[-0.2728, 0.0057]	0.1235	[-0.0156, 0.2625]	**0.1674**	[0.0289, 0.3059]	-0.0165	[-0.0557, 0.0062]	-9.9

https://doi.org/10.5194/egusphere-2026-4384
Preprint. Discussion started: 4 August 2026

Lag time (day)	a	95% CI	b	95% CI	c	95% CI	a×b	95% CI	Contribution rates(%)
3	0.1034	[-0.0364, 0.2432]	**-0.3458**	[-0.4783, -0.2133]	-0.0800	[-0.2201, 0.0600]	-0.0358	[-0.0869, 0.0177]	44.7
4	**0.2076**	[0.0514, 0.3638]	**-0.3356**	[-0.4849, -0.1863]	**0.2489**	[0.0942, 0.4035]	**-0.0697**	[-0.1365, -0.0104]	-28.0
5	0.0542	[-0.1381, 0.2465]	-0.0451	[-0.2368, 0.1466]	0.1391	[-0.0516, 0.3298]	-0.0024	[-0.0277, 0.0169]	-1.8
6	-0.0842	[-0.2565, 0.0880]	0.0291	[-0.1450, 0.2031]	0.0172	[-0.1557, 0.1900]	-0.0024	[-0.0253, 0.0152]	-14.3
7	-0.2088	[-0.4550, 0.0374]	0.1481	[-0.1034, 0.3997]	-0.2000	[-0.4467, 0.0466]	-0.0309	[-0.1447, 0.0265]	15.5
8	0.0696	[-0.1816, 0.3207]	-0.1006	[-0.3538, 0.1526]	0.0121	[-0.2397, 0.2638]	-0.0070	[-0.0333, 0.0240]	-57.9
9	-0.3011	[-0.6777, 0.0754]	**-0.5228**	[-0.8379, -0.2078]	**-0.4428**	[-0.7968, -0.0887]	0.1574	[-0.0360, 0.3287]	-35.6
10	0.1454	[-0.1387, 0.4294]	-0.0507	[-0.3116, 0.2102]	**-0.4542**	[-0.7100, -0.1984]	-0.0074	[-0.0616, 0.0272]	1.6
11	**-0.4329**	[-0.6432, -0.2226]	**-0.2192**	[-0.4169, -0.0214]	**-0.6207**	[-0.8036, -0.4378]	**0.0949**	[0.0112, 0.1776]	-15.3
12	**-0.3813**	[-0.5748, -0.1877]	0.0338	[-0.1487, 0.2164]	**-0.5977**	[-0.7656, -0.4298]	-0.0129	[-0.0924, 0.0475]	2.2
13	-0.1350	[-0.3954, 0.1254]	-0.1326	[-0.3802, 0.1151]	**-0.3561**	[-0.6017, -0.1105]	0.0179	[-0.0185, 0.1348]	-5.0
14	**-0.4941**	[-0.6684, -0.3198]	0.0466	[-0.1559, 0.2492]	**-0.4845**	[-0.6599, -0.3091]	-0.0230	[-0.1236, 0.0859]	4.8
15	0.3121	[-0.0359, 0.6601]	-0.1634	[-0.5408, 0.2140]	0.2265	[-0.1303, 0.5833]	-0.0510	[-0.2340, 0.0620]	-22.5
16	-0.2390	[-0.5306, 0.0525]	0.0139	[-0.2286, 0.2565]	**-0.6317**	[-0.8645, -0.3990]	-0.0033	[-0.0467, 0.0783]	0.5

https://doi.org/10.5194/egusphere-2026-4384
Preprint. Discussion started: 4 August 2026

Lag time (day)	a	95% CI	b	95% CI	c	95% CI	a×b	95% CI	Contribution rates(%)
17	0.2704	[-0.1449, 0.6857]	**-0.4743**	[-0.8802, -0.0685]	0.1021	[-0.3270, 0.5312]	-0.1283	[-0.3526, 0.0089]	-125.6
18	-0.0171	[-0.3073, 0.2730]	-0.1973	[-0.4821, 0.0876]	0.1383	[-0.1491, 0.4257]	0.0034	[-0.0755, 0.0772]	2.4
19	**-0.6876**	[-0.9935, -0.3817]	**0.4395**	[0.1741, 0.7050]	**-0.8357**	[-1.0671, -0.6044]	**-0.3022**	[-0.7667, -0.0982]	36.2
20	0.3648	[-0.0695, 0.7991]	0.1640	[-0.2191, 0.5471]	**-0.6518**	[-1.0055, -0.2981]	0.0598	[-0.0873, 0.1816]	-9.2
21	—	—	—	—	—	—	—	—	—

Note: Bold values indicate significant indirect effects (95% CI not crossing zero). Data for Lag 21 are not shown due to insufficient sample size.

Table A3. Mediating effects of EKE on Chl-a via temperature fronts within the eddy core (0-1R) of ACEs

Lag time (day)	a	95% CI	b	95% CI	c	95% CI	a×b	95% CI	Contribution rates(%)
0	**0.1000**	[0.0535, 0.1466]	**0.2597**	[0.2145, 0.3049]	**-0.1056**	[-0.1521, -0.0591]	**0.0260**	[0.0145, 0.0413]	-24.6
1	**0.1912**	[0.1172, 0.2651]	**0.1197**	[0.0434, 0.1960]	0.0250	[-0.0503, 0.1004]	**0.0229**	[0.0078, 0.0428]	91.4
2	0.0894	[-0.0001, 0.1789]	**0.3612**	[0.2769, 0.4454]	-0.0084	[-0.0982, 0.0815]	**0.0323**	[0.0025, 0.0634]	-385.9
3	**0.2691**	[0.1784, 0.3597]	**0.2181**	[0.1227, 0.3135]	0.0758	[-0.0181, 0.1696]	**0.0587**	[0.0193, 0.1138]	77.5
4	**0.2700**	[0.1685, 0.3715]	**0.3524**	[0.2492, 0.4555]	-0.0223	[-0.1277, 0.0831]	**0.0951**	[0.0395, 0.1681]	-427.1
5	**0.3677**	[0.2435, 0.4918]	**0.2444**	[0.1057, 0.3831]	**-0.1388**	[-0.2710, -0.0066]	**0.0899**	[0.0182, 0.1929]	-64.8
6	**0.4690**	[0.3491, 0.5888]	**0.2057**	[0.0619, 0.3496]	**-0.3077**	[-0.4368, -0.1786]	**0.0965**	[0.0065, 0.2149]	-31.4

https://doi.org/10.5194/egusphere-2026-4384
Preprint. Discussion started: 4 August 2026

Lag time (day)	a	95% CI	b	95% CI	c	95% CI	a×b	95% CI	Contribution rates(%)
7	**0.6185**	[0.5042, 0.7328]	**0.3477**	[0.1750, 0.5204]	**-0.2440**	[-0.3851, -0.1030]	**0.2150**	[0.1128, 0.3489]	-88.1
8	**0.2297**	[0.0507, 0.4087]	-0.0658	[-0.2514, 0.1199]	**-0.1981**	[-0.3784, -0.0179]	-0.0151	[-0.0584, 0.0259]	7.6
9	**0.6835**	[0.5429, 0.8241]	**0.2756**	[0.0167, 0.5346]	-0.0729	[-0.2649, 0.1192]	**0.1884**	[0.0100, 0.4551]	-258.6
10	**0.7553**	[0.6196, 0.8910]	-0.1105	[-0.4271, 0.2061]	0.0455	[-0.1613, 0.2524]	-0.0834	[-0.2546, 0.0878]	-183.3
11	**-0.2843**	[-0.4851, -0.0836]	**-0.4070**	[-0.6091, -0.2049]	-0.0388	[-0.2480, 0.1705]	**0.1157**	[0.0604, 0.2512]	-298.4
12	**-0.2454**	[-0.4520, -0.0388]	-0.0658	[-0.2863, 0.1547]	0.0384	[-0.1746, 0.2513]	0.0161	[-0.0249, 0.0646]	42.1
13	**-0.2179**	[-0.4271, -0.0087]	-0.1726	[-0.3809, 0.0357]	**0.2880**	[0.0827, 0.4933]	**0.0376**	[0.0062, 0.0805]	13.1
14	**-0.3077**	[-0.4928, -0.1227]	-0.1777	[-0.3712, 0.0158]	**0.2899**	[0.1038, 0.4760]	**0.0547**	[0.0106, 0.1189]	18.9
15	**-0.4709**	[-0.6497, -0.2922]	-0.2250	[-0.4507, 0.0008]	-0.0689	[-0.2710, 0.1332]	**0.1059**	[0.0138, 0.2196]	-153.8
16	**-0.4847**	[-0.7234, -0.2461]	-0.2318	[-0.5379, 0.0743]	-0.1193	[-0.3902, 0.1515]	0.1124	[-0.0669, 0.3370]	-94.2
17	**-0.4434**	[-0.7609, -0.1260]	-0.1767	[-0.5701, 0.2168]	-0.1256	[-0.4770, 0.2258]	0.0783	[-0.0668, 0.2627]	-62.4
18	**-0.2703**	[-0.4604, -0.0803]	-0.0209	[-0.2121, 0.1703]	**0.3720**	[0.1888, 0.5553]	0.0056	[-0.0463, 0.0425]	1.5
19	**-0.2773**	[-0.4689, -0.0857]	0.1831	[-0.0219, 0.3881]	-0.0585	[-0.2576, 0.1406]	**-0.0508**	[-0.1180, -0.0014]	86.8
20	**-0.3756**	[-0.6362, -0.1151]	-0.2126	[-0.5119, 0.0866]	0.0886	[-0.1914, 0.3686]	**0.0799**	[0.0069, 0.2310]	90.1

https://doi.org/10.5194/egusphere-2026-4384
Preprint. Discussion started: 4 August 2026

Lag time (day)	a	95% CI	b	95% CI	c	95% CI	a×b	95% CI	Contribution rates(%)
21	0.0758	[-0.1296, 0.2811]	-0.0562	[-0.2629, 0.1504]	0.0805	[-0.1247, 0.2858]	-0.0043	[-0.0440, 0.0052]	-5.3

Note: Bold values indicate significant indirect effects (95% CI not crossing zero).

Table A4. Mediating effects of relative vorticity on Chl-a via temperature fronts within the eddy core (0-1R) of ACEs

Lag time (day)	a	95% CI	b	95% CI	c	95% CI	a×b	95% CI	Contribution rates(%)
0	-0.0334	[-0.0802, 0.0133]	**0.2441**	[0.1989, 0.2894]	**-0.0802**	[-0.1268, -0.0335]	-0.0082	[-0.0197, 0.0012]	10.2
1	**-0.1176**	[-0.1924, -0.0428]	**0.1164**	[0.0411, 0.1918]	-0.0450	[-0.1203, 0.0303]	**-0.0137**	[-0.0265, -0.0023]	30.4
2	**-0.1793**	[-0.2677, -0.0908]	**0.3597**	[0.2743, 0.4451]	-0.0524	[-0.1421, 0.0374]	**-0.0645**	[-0.0959, -0.0365]	123.1
3	**-0.2279**	[-0.3196, -0.1363]	**0.2178**	[0.1235, 0.3121]	-0.0711	[-0.1650, 0.0228]	**-0.0496**	[-0.0921, -0.0190]	69.8
4	**-0.1268**	[-0.2313, -0.0222]	**0.3294**	[0.2289, 0.4300]	0.0275	[-0.0779, 0.1329]	**-0.0418**	[-0.1000, -0.0035]	-151.9
5	-0.0136	[-0.1471, 0.1199]	**0.1617**	[0.0302, 0.2931]	0.0946	[-0.0383, 0.2275]	-0.0022	[-0.0394, 0.0311]	-2.3
6	**0.2208**	[0.0884, 0.3531]	0.0097	[-0.1297, 0.1491]	0.0315	[-0.1041, 0.1672]	0.0021	[-0.0336, 0.0471]	6.8
7	**0.1560**	[0.0124, 0.2997]	0.0740	[-0.0730, 0.2211]	-0.0542	[-0.1994, 0.0911]	0.0115	[-0.0027, 0.0344]	-21.3
8	**-0.2209**	[-0.4002, -0.0415]	-0.0603	[-0.2443, 0.1238]	**0.2286**	[0.0495, 0.4076]	0.0133	[-0.0219, 0.0475]	5.8
9	**0.3890**	[0.2116, 0.5664]	0.1437	[-0.0641, 0.3515]	-0.0640	[-0.2562, 0.1282]	0.0559	[-0.0275, 0.1691]	-87.3

https://doi.org/10.5194/egusphere-2026-4384
Preprint. Discussion started: 4 August 2026

Lag time (day)	a	95% CI	b	95% CI	c	95% CI	a×b	95% CI	Contribution rates(%)
10	**0.3133**	[0.1167, 0.5099]	-0.0766	[-0.2917, 0.1386]	0.1787	[-0.0250, 0.3825]	-0.0240	[-0.0796, 0.0188]	-13.4
11	-0.0815	[-0.2902, 0.1272]	**-0.3573**	[-0.5536, -0.1610]	0.0997	[-0.1087, 0.3081]	0.0291	[-0.0360, 0.0979]	29.2
12	-0.1516	[-0.3622, 0.0590]	-0.0412	[-0.2533, 0.1709]	0.2045	[-0.0041, 0.4131]	0.0062	[-0.0395, 0.0416]	3.1
13	**-0.2414**	[-0.4494, -0.0334]	**-0.2428**	[-0.4588, -0.0268]	-0.0063	[-0.2206, 0.2081]	**0.0586**	[0.0100, 0.1379]	-933.9
14	0.0101	[-0.1843, 0.2046]	**-0.2486**	[-0.4356, -0.0616]	-0.1503	[-0.3426, 0.0419]	-0.0025	[-0.0560, 0.0362]	1.7
15	0.1503	[-0.0500, 0.3506]	-0.1485	[-0.3523, 0.0553]	0.0167	[-0.1858, 0.2193]	-0.0223	[-0.0761, 0.0118]	-133.6
16	**0.5743**	[0.3509, 0.7976]	-0.1249	[-0.4590, 0.2093]	-0.0624	[-0.3347, 0.2099]	-0.0717	[-0.3692, 0.1976]	115.0
17	-0.1242	[-0.4756, 0.2272]	-0.0789	[-0.4398, 0.2820]	0.0694	[-0.2839, 0.4227]	0.0098	[-0.0537, 0.1161]	14.1
18	0.0681	[-0.1288, 0.2651]	-0.1151	[-0.3120, 0.0819]	-0.0796	[-0.2763, 0.1172]	-0.0078	[-0.0510, 0.0240]	9.9
19	-0.0236	[-0.2230, 0.1758]	0.1813	[-0.0129, 0.3754]	-0.1724	[-0.3689, 0.0240]	-0.0043	[-0.0363, 0.0348]	2.5
20	0.1246	[-0.1543, 0.4036]	-0.2211	[-0.5004, 0.0582]	0.0139	[-0.2671, 0.2950]	-0.0276	[-0.1082, 0.0161]	-197.6
21	**-0.2363**	[-0.4364, -0.0362]	-0.0115	[-0.2217, 0.1987]	0.1648	[-0.0383, 0.3679]	0.0027	[-0.0074, 0.0165]	1.6

Note: Bold values indicate significant indirect effects (95% CI not crossing zero).

https://doi.org/10.5194/egusphere-2026-4384
Preprint. Discussion started: 4 August 2026

Author contributions

Aoran Sun: Conceptualization, Methodology, Writing- Original draft preparation.
Chunling Zhang: Writing- Original draft preparation, Corresponding author.
Huangxin Yang: Data curation, Investigation.
Yuntao Zhou: Conceptualization, Reviewing and Editing, Corresponding author.

Competing interests

The contact author has declared that none of the authors has any competing interests.

Disclaimer

Publisher's note: Copernicus Publications remains neutral with regard to jurisdictional claims in published maps and institutional affiliations.

Acknowledgements

The authors are grateful to the Copernicus Marine Service for the satellite remote sensing data. We also acknowledge all the colleagues and project members who have contributed to the sea experiments, and data processing in the past. Many scientists, engineers, and students have actively participated in surveys and mappings.

Financial support

This study was financially supported in part by the General Program of the National Natural Science Foundation of China under Grant 42576203, and in part by the Program on the Survey, Monitoring and Assessment of Global Fishery Resources (Comprehensive scientific survey of fisheries resources at the high seas) sponsored by the Ministry of Agriculture and Rural Affairs under Grant D-8025-25-5001-02.

References

Belkin, I.M., and O'Reilly, J.E.: An algorithm for oceanic front detection in chlorophyll and SST satellite imagery, J. Mar. Syst. 78, 319–326, https://doi.org/10.1016/j.jmarsys.2008.11.018, 2009.

Belkin, I.M., Cornillon, P.C., and Sherman, K.: Fronts in large marine ecosystems, Prog. Oceanogr., 81, 223–236, https://doi.org/10.1016/j.pocean.2009.04.015, 2009.

Bjornsson, H. and Venegas, S. A.: A Manual for EOF and SVD Analyses of Climatic Data, Centre for Climate and Global Change Research, Sydney, 112–134, 1997.

Calil, P.H.R., and Richards, K.J.: Transient upwelling hot spots in the oligotrophic North Pacific, J. Geophys. Res. Oceans, 115, C02003, https://doi.org/10.1029/2009JC005360,2010.

Canny, J.: A computational approach to edge detection, IEEE Trans. Pattern Anal. Mach. Intell., 8, 679–698, https://doi.org/10.1109/TPAMI.1986.4767851, 1986.

Chaigneau, A., Eldin, G., and Dewitte, B.: Eddy activity in the four major upwelling systems from satellite altimetry (1992–2007), Prog. Oceanogr., 83, 117–123, https://doi.org/10.1016/j.pocean.2009.07.012, 2009.

Chelton, D.B., Schlax, M.G., and Samelson, R.M.: Global observations of nonlinear mesoscale eddies, Prog. Oceanogr., 91, 167–216, https://doi.org/10.1016/j.pocean.2011.01.002,2011.

Chu, P.C., and Wang, G.H.: Seasonal Variability of Thermohaline Front in the Central South China Sea, J. Oceanogr., 59, 65–78, https://doi.org/10.1023/A:1022868407012, 2003.

Copernicus Marine Environment Monitoring Service (CMEMS): Global Ocean Colour (Copernicus-GlobColour), Bio-Geo-Chemical, L4 (daily) from Satellite Observations, CMEMS [data set], https://doi.org/10.48670/moi-00281, 2024.

Gaube, P., McGillicuddy, D.J., Chelton, D.B., Behrenfeld, M.J., and Strutton, P.G.: Regional variations in the influence of mesoscale eddies on near-surface chlorophyll, J. Geophys. Res. Oceans, 119, 8195–8220, https://doi.org/10.1002/2014JC010111, 2014.

Guo, M.X., Xiu, P., and Xing, X.G.: Oceanic fronts structure phytoplankton distributions in the central South Indian Ocean, J. Geophys. Res. Oceans, 127, e2021JC017594, https://doi.org/10.1029/2021JC017594, 2022.

JPL MUR MEaSUREs Project: GHRSST Level 4 MUR Global Foundation Sea Surface Temperature Analysis, Ver. 4.1, PO.DAAC [data set], https://doi.org/10.5067/GHGMR-4FJ04, 2022.

Kim, B., Kim, S., Kwon, S., Lee, S., and Kim, E.: Seasonal frontal variability and stratification coupling from 2022 CTD observations in the southern coastal waters of Korea, Front. Mar. Sci., 12, 1723724, https://doi.org/10.3389/fmars.2025.1723724, 2025.

Lellouche, J. M., Greiner, E., Bourdallé-Badie, R., Garric, G., Melet, A., Drévillon, M., Bricaud, C., Hamon, M., Le Galloudec, O., Regnier, C., and Le Traon, P. Y.: The Copernicus Global 1/12° Oceanic and Sea Ice GLORYS12 Reanalysis, Front. Earth Sci., 9, 698876, https://doi.org/10.3389/feart.2021.698876, 2021.

Liu, Y., Dong, C.M., Guan, Y.P., Chen, D.K., McWilliams, J., and Nencioli, F.: Eddy analysis in the subtropical zonal band of the North Pacific Ocean, Deep-Sea Res. I, 68, 54–67, https://doi.org/10.1016/j.dsr.2012.06.001,2012.

Lu, Y.Y., and Kamenkovich, I.: Mesoscale eddy-induced sharpening of oceanic tracer fronts, J. Adv. Model. Earth Syst., 17, e2024MS004693, https://doi.org/10.1029/2024MS004693, 2025.

McGillicuddy, D.J.: Mechanisms of physical-biological-biogeochemical interaction at the oceanic mesoscale, Ann. Rev. Mar. Sci., 8, 125–159, https://doi.org/10.1146/annurev-marine-010814-015606, 2016.

McWilliams, J.C.: Oceanic Frontogenesis, Ann. Rev. Mar. Sci., 13, 227-253, https://doi.org/10.1146/annurev-marine-032320-120725, 2021.

Moline, M. A.: Offshore fronts potentially drive variability in phytoplankton production in the NE Pacific, AGU Fall Meeting 2014, San Francisco, CA, 15–19 December 2014, 2014.

Naveira Garabato, A.C., Ferrari, R., and Polzin, K.L.: Eddy stirring in the Southern Ocean, J. Geophys. Res., 116, C09019, https://doi.org/10.1029/2010JC006818, 2011.

Nencioli, F., Dong, C.M., Dickey, T., Washburn, L., and McWilliams, J.C.: A vector geometry-based eddy detection algorithm and its application to a high-resolution numerical model product and high-frequency radar surface velocities in the Southern California Bight, J. Atmos. Oceanic Technol., 27, 564–579, https://doi.org/10.1175/2009JTECHO725.1, 2010.

Ping, B., Su, F.Z., Meng, Y.S., Fang, S.H., and Du, Y.Y.: A model of sea surface temperature front detection based on a threshold interval, Acta Oceanol. Sin., 33, 65–71, https://doi.org/10.1007/s13131-014-0502-x, 2014.

Preacher, K.J., and Hayes, A.F.: SPSS and SAS procedures for estimating indirect effects in simple mediation models, Behav. Res. Methods Instrum. Comput., 36, 717–731, https://doi.org/10.3758/BF03206553, 2004.

Qiu, B., Chen, S.M., Klein, P., Sasaki, H., and Sasai, Y.: Seasonal mesoscale and submesoscale eddy variability along the North Pacific Subtropical Countercurrent, J. Phys. Oceanogr., 44, 3079–3098, https://doi.org/10.1175/JPO-D-14-0071.1, 2014.

Ribbe, J., Toaspern, L., Wolff, J.O., and Ismail, M.F.A.: Frontal eddies along a western boundary current, Cont. Shelf Res., 165, 51–59, https://doi.org/10.1016/j.csr.2018.06.007, 2018.

Sasai, Y., Sasaoka, K., Sasaki, H., and Ishida, A.: Seasonal and intraseasonal variability of chlorophyll-a in the North Pacific: model and satellite data, J. Geophys. Res., 8, 3–11, 2010.

Siegel, D.A., Peterson, P., McGillicuddy, D.J., Maritorena, S., and Nelson, N.B.: Bio-optical footprints created by mesoscale eddies in the Sargasso Sea, Geophys. Res. Lett., 38, L13608, https://doi.org/10.1029/2011GL047660, 2011.

Sobel, I., and Feldman, G.: A 3x3 isotropic gradient operator for image processing, Stanford Artificial Intelligence Laboratory (SAIL), Stanford, 1968.

Tang, R., Yu, Y., Xi, J.Y., Ma, W.T., and Wang, Y.T.: Mesoscale eddies induce variability in the sea surface temperature gradient in the Kuroshio Extension, Front. Mar. Sci., 9, 926954, https://doi.org/10.3389/fmars.2022.926954, 2022.

Taylor, J.R., and Ferrari, R.: Ocean fronts trigger high latitude phytoplankton blooms, Geophys. Res. Lett., 38, L23601, https://doi.org/10.1029/2011GL049312, 2011.

Ueno, H., Crawford, W.R., and Onishi, H.: Impact of Alaskan Stream eddies on chlorophyll distribution in the North Pacific, J. Oceanogr., 66, 319–328, https://doi.org/10.1007/s10872-010-0028-6, 2010.

Vlasenko, V., Stashchuk, N., and Hutter, K.: Baroclinic Tides: Theoretical Modeling and Observational Evidence, Cambridge University Press, Cambridge, 104–145, 2005.

Wilks, D.S.: Statistical Methods in the Atmospheric Sciences. Elsevier, Amsterdam, 2011.

Woodson, C.B., and Litvin, S.Y.: Ocean fronts drive marine fishery production and biogeochemical cycling, Proc. Natl. Acad. Sci., 112 1710–1715, https://doi.org/10.1073/pnas.1417143112, 2015.

Wu, B.Y., and Jing, Z.Y.: Wind variability at synoptic-to-planetary frequencies enhances front asymmetry of mesoscale eddy, J. Phys. Oceanogr., 56 , 1197–1213, https://doi.org/10.1175/JPO-D-25-0203.1, 2026.

Xing, Q.W., Yu, H.Q., and Wang, H.: Global mapping and evolution of persistent fronts in Large Marine Ecosystems over the past 40 years, Nat. Commun., 15, 4090, https://doi.org/10.1038/s41467-024-48566-w, 2014.

Yu, Y., Xing, X.G., Liu, H.L., Yuan, Y.P., Wang, Y.T., and Chai, F.: The variability of chlorophyll-a and its relationship with dynamic factors in the basin of the South China Sea, J. Mar. Syst., 200, 103230, https://doi.org/10.1016/j.jmarsys.2019.103230, 2019.

Zhang, Z.G., Qiu, B., Klein, P., and Travis, S.: The influence of geostrophic strain on oceanic ageostrophic motion and surface chlorophyll, Nat. Commun., 10, 2838, https://doi.org/10.1038/s41467-019-10883-w, 2019.